Journal of Alloys and Compounds 506 (2010) 678–682

Contents lists available at ScienceDirect

Journal of Alloys and Compounds

journal homepage: www.elsevier.com/locate/jallcom

Semiconducting properties of Ge-doped $BaSnO_3$ ceramic

Roberto Köferstein [a], Fahrettin Yakuphanoglu [b,*]

[a] Institut für Chemie, Anorganische Chemie, Martin-Luther-Universität Halle-Wittenberg, Kurt-Mothes Strasse 2, D-06120 Halle, Germany
[b] Physics Department, Faculty of Science, Firat University, 23119 Elazığ, Turkey

ARTICLE INFO

Article history:
Received 19 February 2010
Received in revised form 5 July 2010
Accepted 7 July 2010
Available online 15 July 2010

Keywords:
Electrical conductivity
Optical properties
Sintering
Perovskite

ABSTRACT

The electrical and optical properties of Ge-doped $BaSnO_3$ ceramics sintered at various temperatures have been investigated to determine their semiconductor behavior. The electrical conductivity of Ge-doped $BaSnO_3$ samples increases with increase in temperature, confirming that the samples exhibit a semiconductor behavior. A maximum conductivity value of 6.31×10^{-9} S/cm was observed for the sample sintered at 1200 °C. The optical band gaps of the Ge-doped $BaSnO_3$ samples were determined by means of reflectance spectra. The variation of optical band gap with temperature was analyzed using $E_g(T) = E_{go} + \beta T$ relation. The rate of change of the band gap β of $BaSn_{0.99}Ge_{0.01}O_3$ was found to be 7.6×10^{-4} (eV/°C). A minimum optical band gap value of 2.95 eV was observed for the sample sintered at 1400 °C. It is evaluated that $BaSn_{0.99}Ge_{0.01}O_3$ is a wide band gap semiconductor and its semiconducting properties change with sintering temperature.

1. Introduction

Pure and doped barium stannate as well as its solid solutions (e.g. $BaTi_{1-x}Sn_xO_3$) have found important applications in materials science and technology due to their dielectric properties, semiconducting behaviors and high thermal stability. Because of these characteristic properties, $BaSnO_3$ based ceramics are becoming more and more important in material technology. It can be used to prepare thermally stable capacitors and to fabricate ceramic boundary layer capacitors [1–8]. Moreover, barium stannate can be also used as a functional material for semiconductor gas sensors [9–15] and photocatalytic applications [16–18]. $BaSnO_3$ crystallises in the perovskite structure and has a band gap of 3.4 eV [19]. It has been observed that an isovalent partial replacement of Sn^{4+} in $BaSnO_3$ by other cations causes a modification in its electrical properties [5,20–22]. In general, compacts on the basis of $BaSnO_3$ reveal only a moderate densification behavior [2,23–26]. Therefore, such ceramic bodies need high sintering temperatures or very long soaking times [7,27,19]. The addition of additives can significantly reduce the sintering temperature due to an improvement of the densification behavior. Wang et al. [28] used SiO_2 as a sintering aid for $BaSnO_3$ ceramics. Sintering additives can influence not only the sintering temperature but also the (di-)electric properties of the final ceramics [29]. Kumar and Choudhary [22] sintered $BaSnO_3$ at 1200 °C adding $BaSiO_3$. They found the formation of solid solutions of the type $BaSn_{1-x}Si_xO_3$ ($x = 0$–0.15). The $BaSn_{1-x}Si_xO_3$ samples show NTCR (negative temperature coefficient of resistance) behavior and a better electrical conduction at elevated temperature than pure $BaSnO_3$ ceramic bodies. $BaGeO_3$ can be also used as a sintering aid to drastically reduce the sintering temperature as reported for $BaTiO_3$-based ceramics [30–32]. Recently, Köferstein et al. [33] sintered $BaSnO_3$ ceramics at very low temperatures adding $BaGeO_3$ and they found a partial solid solubility of $BaGeO_3$ in $BaSnO_3$.

Here we present the results of our investigations on the electrical and optical properties of Ge-doped $BaSnO_3$ ceramics to determine their semiconducting properties.

2. Experimental details

The preparation procedure is described elsewhere [33]. Briefly, a powder with the composition of $BaSn_{0.99}Ge_{0.01}O_3$ was prepared via a conventional mixed-oxide method. Equivalent amounts of $BaCO_3$ (Sabed VL 600, 99.9%, Solvay), SnO_2 (≥99.0%, Merck) and GeO_2 (99.999%, Acros Organics) were milled in a PVC container for 24 h using ZrO_2-balls and propan-2-ol ($m_{powder}:m_{balls}:m_{Propan\text{-}2\text{-}ol} = 1:1:4$). After filtering and drying the mixture was calcined in static air (heating rate 10 K/min) for 2 h at 1150 °C to obtain a powder with a specific surface area of 3.9 m^2/g. Then the calcined powder was milled with ZrO_2-balls and propan-2-ol in a PVC container for 2 h ($m_{powder}:m_{balls} = 1:4$). After filtering and drying the powder was mixed with 5 mass% of a saturated aqueous solution of polyvinyl alcohol (PVA) as a pressing aid. Then the powder was pressed to pellets with a green density of about 3.5 g/cm^3. The pellets were sintered in static air for 1 h at 1200, 1250, 1300 and 1400 °C (heating rate 10 K/min). The theoretical

* Corresponding author. Tel.: +90 424 237000x3621; fax: +90 424 2330062.
E-mail addresses: fyhanoglu@firat.edu.tr, fyhan@hotmail.com (F. Yakuphanoglu).

0925-8388/$ – see front matter © 2010 Elsevier B.V. All rights reserved.
doi:10.1016/j.jallcom.2010.07.041

bulk density of the ceramic bodies was calculated as 7.22 g/cm^3 [34].

X-ray powder diffraction (XRD) patterns were recorded by a STOE STADI MP diffractometer at 20 °C using CoKα_1 radiation. The specific surface area was determined using nitrogen three-point BET (Nova 1000, Quantachrome Corporation). SEM images were recorded with a Philips XL30 ESEM (Environmental Scanning Electron Microscope). The electrical conductivity measurements of the samples were performed using a KEITHLEY 6517A electrometer. The reflectance spectra of the samples were measured using a UV–VIS–NIR 3600 Shimadzu spectrophotometer with an integrating sphere attachment.

3. Results and discussion

3.1. Structural properties of the $BaSn_{0.99}Ge_{0.01}O_3$ ceramics

Recently, Köferstein et al. [33] reported on the system $BaSnO_3$–$BaGeO_3$. They found a limited solid solubility of $BaGeO_3$ in $BaSnO_3$ of the order of 6–7 mol%, because of their different crystal structures. While $BaSnO_3$ appears in the cubic perovskite structure, $BaGeO_3$ crystallizes in two modifications having a pseudowollastonite-type structure and a pyroxene-type structure, respectively [35–37]. X-ray diffraction investigations of the calcined powder as well as the resulting sintered bodies show only the reflection pattern of $BaSnO_3$ as demonstrated in Fig. 1. Therefore, the samples can be described as a solid solution between $BaGeO_3$ and $BaSnO_3$ written by the formula $BaSn_{0.99}Ge_{0.01}O_3$ (Ge^{IV} occupying the Sn^{IV} sites). $BaSn_{0.99}Ge_{0.01}O_3$ ceramics reveal a drastically better sintering behavior than pure $BaSnO_3$ ceramics [23]. An overview of the ceramic bodies is given in Table 1. Sintering at 1200 °C leads to ceramics with relative density of 82% (5.92 g/cm^3). A relative density of 95% (6.83 g/cm^3) is observed at a slightly higher temperature of 1250 °C. After sintering at 1300 and 1400 °C we obtain ceramics with relative densities of 99% [33].

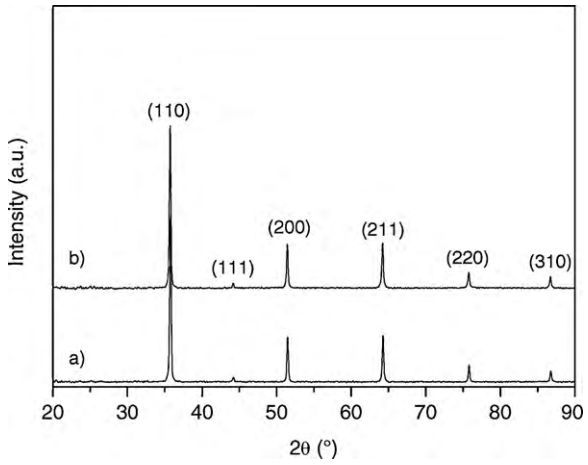

Fig. 1. XRD patterns of the calcined powder (a) and of a ceramic, sintered at 1400 °C for 1 h (b).

Table 1
Structural parameters of the ceramics.

Sintering regime	Relative density[a] (%)	Absolute density (g/cm^3)	Grain size (μm)
1400 °C, 1 h	99	7.18	2.5–26
1300 °C, 1 h	99	7.13	2.5–7 and 0.5–1 (bimodal)
1250 °C, 1 h	95	6.83	0.46–1.5
1200 °C, 1 h	82	5.92	0.25–1

[a] Related to the theoretical density of 7.22 g/cm^3.

SEM images of the surface of the ceramic bodies are shown in Fig. 2. Ceramics sintered at 1200 °C exhibit cubical-shaped grains between about 0.25 and 1 μm. Sintering at 1250 °C leads only to a moderate grain growth between 0.45 and 1.5 μm. A further increasing sintering temperature to 1300 °C causes a bimodal grain growth with grain fractions between about 0.5–1 and 2.5–7 μm.

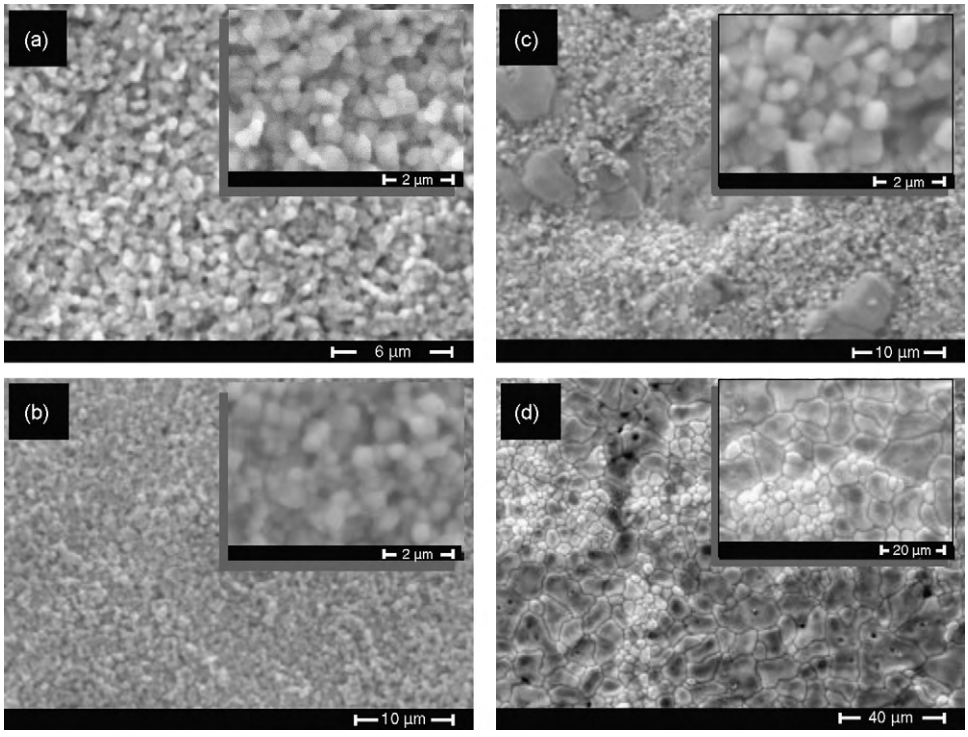

Fig. 2. SEM images of the ceramic bodies sintered at various temperatures for 1 h. (a) 1200 °C, (b) 1250 °C, (c) 1300 °C, (d) 1400 °C.

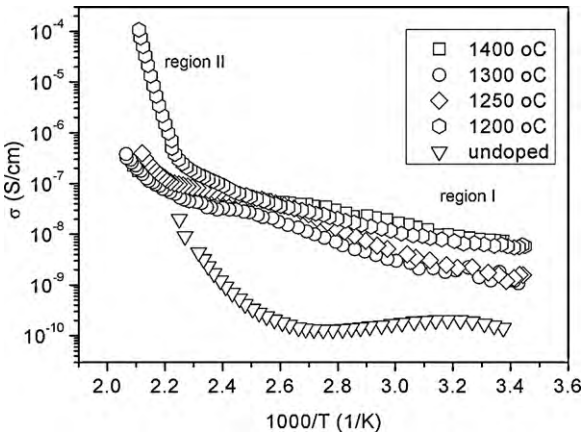

Fig. 3. Plots of electrical conductivity plots of the ceramics sintered at various temperatures.

The smaller grain fraction has cubical-shaped grains, whereas the larger grain fraction shows grains with a more irregular shape. At 1400 °C we obtain bodies with a heterogeneous grain distribution between 2.5 and 26 μm (see also Ref. [33]).

3.2. Electrical conductivity of the $BaSn_{0.99}Ge_{0.01}O_3$ ceramics

Fig. 3 shows electrical conductivity plots of undoped $BaSnO_3$ and sintered $BaSn_{0.99}Ge_{0.01}O_3$ ceramics. As seen in Fig. 3, the electrical conductivity of undoped $BaSnO_3$ sample is lower than that of doped sample. This suggests that the electrical conductivity of undoped $BaSnO_3$ increases with Ge dopant. The electrical conductivity of the samples increases with temperature, confirming that the samples exhibit the semiconductor behavior. The electrical conductivity plots show two linear regions (I and II) corresponding to various conduction mechanisms. The first region shows a linear at lower temperatures ($T < 410$ °C) and second region followed a linear variation at higher temperature ($T > 450$ °C). The electrical conductivity behavior of the ceramics were analyzed using the following relation:

$$\sigma = \sigma_o \exp\left(-\frac{\Delta E}{kT}\right) \quad (1)$$

where σ_o is the pre-exponential factor, E is the activation energy, k is the Boltzmann constant. The activation energy values for I and II regions, E_I and E_{II}, were determined from the slope of Fig. 3 and are given in Table 2. The electrical conductivity values of ceramics at 25 °C do not indicate a regular trend with sintering temperature. The ceramic sample sintered at 1200 °C shows the highest conductivity. Comparing the electrical conductivity values of the samples with respect to sintering temperature, we evaluate that the grain size is an effective parameter in the conduction mechanism of the samples and the sample of the smallest grain size shows the highest conductivity. This shows that when the grain size was reduced to the nanometric regime, the electrical conductivity could be greatly enhanced.

The electrical conductivity of the samples sintered at 1400, 1300 and 1250 °C is lower than that of calcium modified $BaSnO_3$, whereas the electrical conductivity of the sample sintered at 1200 °C is higher than that of it [38]. The activation energy values of the samples for first (except for 1200 °C) and second regions decrease with increasing sintering temperatures. The samples sintered at 1250 and 1200 °C have the higher activation energy values, 1.280 and 3.177 eV, respectively. This is attributed to long range diffusion of doubly ionized oxygen vacancies $V_o^{\bullet\bullet}$ in present perovskite oxides [39,40]. Whereas, the activation energy values of the samples sintered at 1300 and 1400 °C is lower than that of the samples sintered at 1250 and 1200 °C, respectively. The long range diffusion of doubly ionized oxygen vacancies V_O changes with increasing annealed temperatures.

Table 2
Electrical parameters of the ceramics.

Sint. temp.	E_g (eV)	E_I (eV)	E_{II} (eV)	σ (S/cm)
1400 °C, 1 h	2.95	0.223	0.518	4.54×10^{-10}
1300 °C, 1 h	3.03	0.356	0.889	1.08×10^{-10}
1250 °C, 1 h	3.07	0.415	1.280	1.10×10^{-10}
1200 °C, 1 h	3.1	0.264	3.177	6.31×10^{-9}

3.3. Optical properties of the $BaSn_{0.99}Ge_{0.01}O_3$ ceramics

Fig. 4a shows the reflectance spectra of the samples sintered at various temperatures. It is seen that the samples have high reflectance in the visible range of 400–700 nm. The optical band gap of samples can be determined by the following relation [41]:

$$\alpha h\nu = A(h\nu - E_g)^n \quad (2)$$

where α is the absorption coefficient, A is an energy-independent constant and E_g is the optical band gap. n is a constant which determines the type of optical transitions and for indirect allowed transition, $n = 2$ and indirect forbidden transition, $n = 3$, for direct allowed transition, $n = 1/2$; for direct forbidden transition, $n = 3/2$. In order to determine optical band gaps of the samples, firstly, the reflectance values were converted to absorbance by application of the Kubelka–Munk function [42,43]. Kubelka–Munk theory is generally used for the analysis of diffuse reflectance spectra obtained from weakly absorbing samples. The optical band gap of lanthanum-doped stannate $BaSnO_3$ has been determined using diffuse reflectance spectra [44]. Kubelka–Munk formula for determination of optical band gap of $BaSnO_3$ ceramics is expressed by the following relation:

$$F(R) = \frac{(1-R)^2}{2R} \quad (3)$$

where R is the reflectance, $F(R)$ is the Kubelka–Munk function corresponding absorbance and α is determined using $\alpha = F(R)/d$, here d is the thickness. The transmittance spectra of the ceramic sintered were obtained by means of Kubelka–Munk formula and are shown in Fig. 4b. The transmittance of the ceramic samples decreases with increasing sintering temperature. The sample sintered at 1250 °C indicates the highest transparency. The transmittance of the samples changes with sintered temperature and indicates an absorption edge. The absorption edge varies with increasing sintering temperature, suggesting that the optical band gap changes with the temperature.

For determination of nature of the optical transitions, we have to find n value. For this, Eq. (2) can be written in the following form [45]:

$$\ln \alpha = \ln A - \ln(h\nu) + n \ln(h\nu - E_g) \quad (4)$$

In this equation, firstly, the approximate value of the optical band gap must be determined. When E_g is found, the value of r can be determined from the slope of $\ln(h\nu)$ as a function of $\ln(h\nu - E_g)$. If $(d(\ln \alpha)/d(h\nu))$ is plotted as a function of $(h\nu)$ for the compound, $d(\ln \alpha)/d(h\nu) = f(h\nu)$ will show a maximum value corresponding to approximate value of the optical band gap [46]. After determination of approximate value of the optical band gap, the value of n is determined from the slope of $\ln(h\nu)$ vs. $\ln(h\nu - E_g)$ curve plotted and was found to be about 0.5. This value suggests that the direct transitions are dominant in the samples and Eq. (2) can be therefore

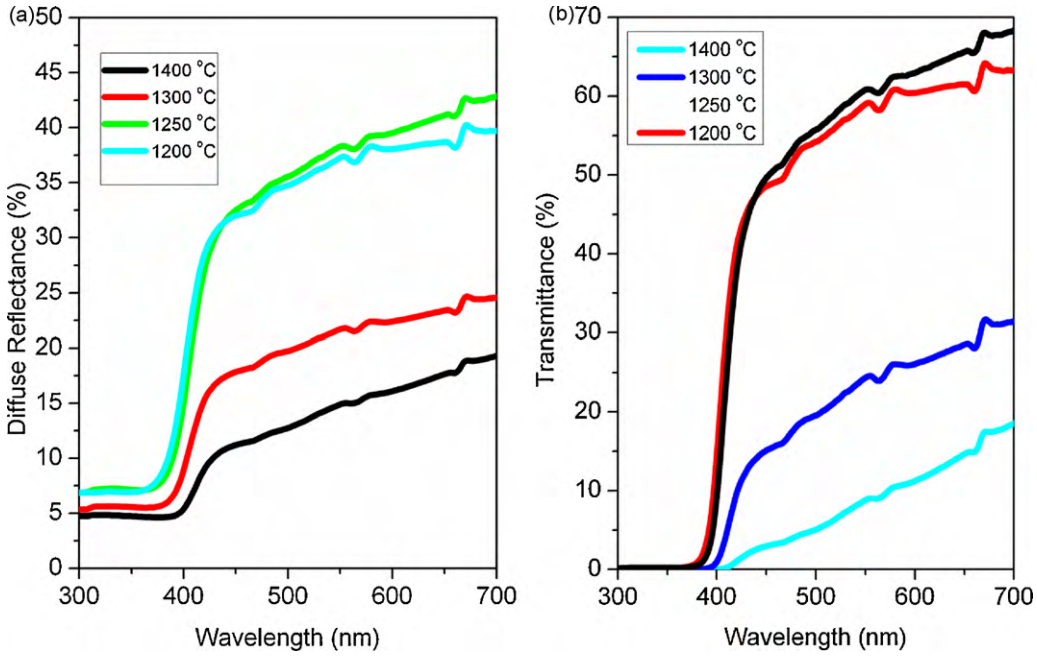

Fig. 4. Transmittance and reflectance spectra of the ceramics sintered at various temperatures.

written as follows:

$$\alpha h\nu = A(h\nu - E_g)^{1/2} \quad (5)$$

The exact optical band gap values of the samples was determined from the plots of $(\alpha h\nu)^2$ vs. $h\nu$, as shown in Fig. 5 and given in Table 2. It is evident from Table 2 that the value of E_g changes with sintering temperature. The obtained bad gap values of the samples are lower than that of $BaSnO_3$, prepared by the mixed-oxide method, which is a wide band gap material having an energy gap of 3.4 eV [19,47]. This suggests that the Ge dopant and sintering temperature decrease the optical band gap. The change in optical band gap with increasing annealing temperature could be attributed to the improved crystalline nature and porosity related to density change of films. The optical band gap of the samples is related to the crystalline nature, which in turn strongly depends on the annealing temperature and density. The E_g values of the samples are linearly decreased with the sintering temperature, as shown in Fig. 6. The linearity change can be expressed [48]:

$$E_g(T) = E_{go} + \beta T \quad (6)$$

where E_{go} is a constant and β is the rate of change of band gap with temperature. The least-square fit of Fig. 6 gives:

$$E_g(T) = -7.6 \times 10^{-4}\, T(^\circ\mathrm{C}) + 4.068 \quad (7)$$

From this relation, the β value for the $BaSn_{0.99}Ge_{0.01}O_3$ was found to be 7.6×10^{-4} (eV/°C). We can evaluate that the decrease in the optical band gap of the $BaSn_{0.99}Ge_{0.01}O_3$ is due to atomic distances changing by temperature. The sample sintered at 1400 °C indicated a minimum optical band gap value of 2.95 eV. The optical band gap of the sample sintered at 1400 °C is lower than that of lanthanum-doped $BaSnO_3$ [44]. It is evaluated that the sintering temperature has an important effect on the optical band gap of $BaSnO_3$.

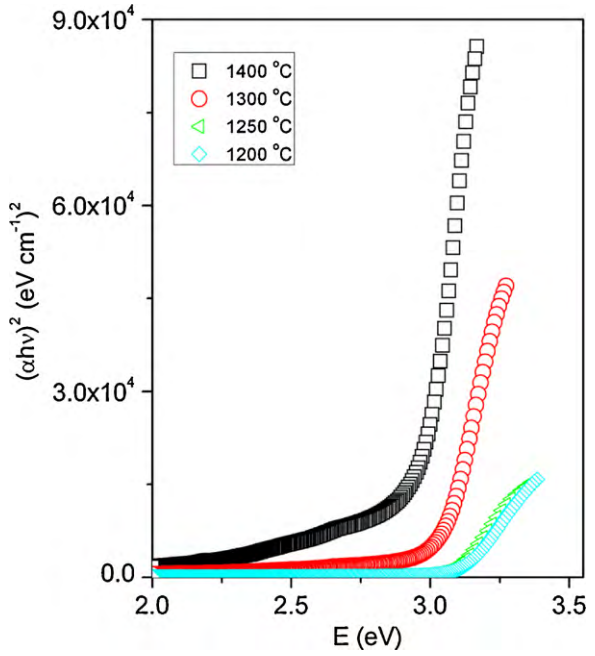

Fig. 5. Plots of $(\alpha h\nu)^2$ vs. $h\nu$ of the ceramics sintered at various temperatures.

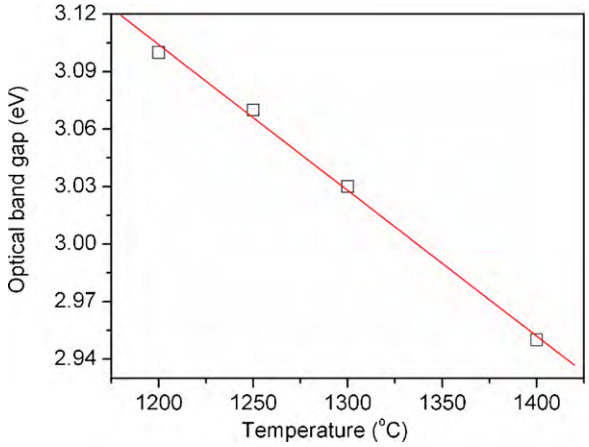

Fig. 6. Plots of E_g vs. T of the ceramics sintered at various temperatures.

4. Conclusions

The semiconducting properties of the Ge-doped $BaSnO_3$ sintered at various temperatures have been investigated. The sintering temperature changed the electrical and optical properties of Ge-doped $BaSnO_3$. The sample sintered at 1200 °C shows the highest electrical conductivity, and also the sample sintered at 1400 °C indicates the lowest band gap.

We have evaluated that $BaSn_{0.99}Ge_{0.01}O_3$ is a wide band gap semiconductor with the determined electronic parameters.

References

[1] R. Vivekanandan, T.R.N. Kutty, Mater. Sci. Eng. B 6 (1990) 221.
[2] P. Singh, B.J. Brandenburg, C.P. Sebastian, P. Singh, S. Singh, D. Kumar, O. Parkash, K. Jpn. J. Appl. Phys. 47 (2008) 3540.
[3] A. Movchikova, O. Malyshkina, G. Suchaneck, G. Gerlach, R. Steinhausen, H.T. Langhammer, C. Pientschke, H. Beige, J. Electroceram. 20 (2008) 43.
[4] T. Wang, X.M. Chen, X.H. Zheng, J. Electroceram. 11 (2003) 173.
[5] A. Kumar, B.P. Singh, R.N.P. Choudhary, A.K. Thakur, Mater. Lett. 59 (2005) 1880.
[6] O.I. Prokopalo, Ferroelectrics 14 (1976) 683.
[7] P. Singh, D. Kumar, O. Parkash, J. Appl. Phys. 97 (2005) 074103.
[8] H. Brauer, Z. Angew. Phys. 29 (1970) 282.
[9] B. Ostrick, M. Fleischer, U. Lampe, H. Meixner, Sens. Actuators B 44 (1997) 601.
[10] S. Tao, F. Gao, X. Liu, O.T. Sørensen, Sens. Actuators B 71 (2000) 223.
[11] S. Hodjati, K. Vaezzadeh, C. Petit, V. Pitchon, A. Kiennemann, Catal. Today 59 (2000) 323.
[12] P. McGeehin, D.E. Williams, Sensing Gaseous Substances. Int. Appl., Patent No. WO 9308467 A1 19930429, 1993.
[13] V. Gopal Reddy, S.V. Manorama, V.J. Rao, J. Mater. Sci. Mater. Electron. 12 (2001) 137.
[14] S. Upadhyay, P. Kavitha, Mater. Lett. 61 (2007) 1912.
[15] J. Cerda, J. Arbiol, G. Dezanneau, R. Diaz, J.R. Morante, Sens. Actuators B 84 (2002) 21.
[16] P.H. Borse, U.A. Joshi, S.M. Ji, J.S. Jang, J.S. Lee, E.D. Jeong, H.G. Kim, Appl. Phys. Lett. 90 (2007) 034103.
[17] Y. Yuan, J. Lv, X. Jiang, Z. Li, T. Yu, Z. Zou, J. Ye, Appl. Phys. Lett. 91 (2007) 094107.
[18] Y. Zhang, H. Zhang, Y. Wang, W.F. Zhang, J. Phys. Chem. C 112 (2008) 8553.
[19] J. Cava, P. Gammel, B. Batlogg, J.J. Krajewski, W.F. Peck Jr., W.L. Rupp Jr., R. Felder, R.B. van Dover, Phys. Rev. B 42 (1990) 4815.
[20] V. Jayaraman, G. Mangamma, T. Gnanasekaran, G. Periaswami, Solid State Ionics 86–88 (1996) 1111.
[21] P.H. Borse, J.S. Lee, H.G. Kim, J. Appl. Phys. 100 (2006) 124915.
[22] A. Kumar, R.N.P. Choudhary, J. Mater. Sci. 42 (2007) 2476.
[23] R. Köferstein, L. Jäger, M. Zenkner, S.G. Ebbinghaus, J. Eur. Ceram. Soc. 29 (2009) 2317.
[24] P. Singh, D. Kumar, O. Parkash, J. Mater. Sci. Mater. Electron. 16 (2005) 145.
[25] X. Wie, X. Yao, Mater. Sci. Eng. B 137 (2007) 184.
[26] A.-M. Azad, N.C. Hon, J. Alloys Compd. 270 (1998) 95.
[27] B. Piercy, Trans. Faraday Soc. 55 (1959) 39.
[28] Z. Wang, F. Zhou, Z. Chen, Dianzi Yuanjian Yu Cailiao 25 (2006) 58.
[29] R. Köferstein, L. Jäger, M. Zenkner, S.G. Ebbinghaus, Mater. Chem. Phys. 119 (2010) 118.
[30] R. Köferstein, L. Jäger, M. Zenkner, T. Müller, H.-P. Abicht, Mater. Chem. Phys. 112 (2008) 531.
[31] M. Zenkner, L. Jäger, R. Köferstein, H.-P. Abicht, Solid State Sci. 10 (2008) 1556.
[32] R. Köferstein, L. Jäger, M. Zenkner, H.-P. Abicht, J. Mater. Sci. 43 (2008) 832.
[33] R. Köferstein, L. Jäger, M. Zenkner, T. Müller, S.G. Ebbinghaus, J. Eur. Ceram. Soc. 30 (2010) 1419.
[34] G.W. Marks, L.A. Monson, Ind. Eng. Chem. 47 (1955) 1611.
[35] F. Liebau, Neues Jahrb. Miner. 94 (1960) 1209.
[36] W. Hilmar, Acta Crystallogr. 15 (1962) 1101.
[37] D.M. Többens, V. Kahlenberg, C. Gspan, G. Kothleitner, Acta Crystallogr. B62 (2006) 1002.
[38] A. Kumara, B.P. Singh, R.N.P. Choudhary, A.K. Thakur, J. Alloys Compd. 394 (2005) 292.
[39] K.W. Browell, O. Mullar, R.H. Doreuies, Mater. Res. Bull. 11 (1976) 1475.
[40] A.E. Paladino, J. Am. Ceram. Soc. 48 (1965) 476.
[41] M.W. Charles, H. Nick Jr., E.S. Gregory, Physical Properties of Semiconductors, Prentice-Hall, Englewood Cliffs, NJ, 1989.
[42] F. Yakuphanoglu, R. Mehrotra, A. Gupta, M. Munoz, J. Appl. Polym. Sci. 114 (2009) 794.
[43] S.I. Boldish, W.B. White, Am. Miner. 83 (1998) 865.
[44] B. Hadjarab, A. Bouguelia, M. Trari, J. Phys. D: Appl. Phys. 40 (2007) 5833.
[45] F. Yakuphanoglu, B.F. Senkal, A. Sarac, J. Electron. Mater. 37 (2008) 930.
[46] F. Yakuphanoglu, M. Arslan, Solid State Commun. 132 (2004) 229.
[47] G. Larramona, C. Gutierrez, I. Pereira, M. Rosa Nunes, F.M.A. da Costa, J. Chem. Soc. Faraday Trans. 85 (1989) 907.
[48] M.W. Charles, H. Nick Jr., E.S. Gregory, Optical Properties, Physical Properties of Semiconductors, Englewood Cliffs, New Jersey, 1989, pp. 218–219.